The Kinematics of Contact with Compliance

David J. Montana *

BBN Systems and Technologies Corp.
70 Fawcett Street
Cambridge, MA 02138

Abstract

The kinematics of contact describe the motion of a point of contact over the surfaces of two contacting objects in response to a relative motion of these objects. In a previous paper [8], I derived equations which embody this relationship when the two objects are assumed to be rigid bodies. In this paper I extend that analysis by dropping the assumption of rigidity. I derive a set of equations, called the compliant contact equations, which model the kinematics of contact with compliance. I then analyze an illustrative example from a theoretical viewpoint and show how results from experiments I performed agree with theory. Finally, I discuss how adding compliance into the model effects the manipulation tasks described in [8].

1 Introduction

The kinematics of contact describe the motion of a point of contact over the surfaces of two contacting objects in response to a relative motion of these objects. Montana [7,8] and Cai and Roth [2] independently derived a set of equations (called the contact equations) which model this relationship assuming the objects are rigid bodies. Not only is this assumption untrue for the physical world, but there are good arguments that a significant amount of compliance in a grasping surface is desirable to aid in the problem of manipulation [4,1]. Human fingertips are compliant, and there are efforts underway to build grasping surfaces which are like human fingertips [1,3].

In this paper, I extend the analysis of the kinematics of contact done in [8] to drop the assumption of rigidity. The results reported here are a refinement and an introduction into the general literature of work first described in [7]. The remainder of this paper is broken into the following sections. Section 2 provides mathematical background consisting mainly of definitions regarding the geometry of surfaces, a subject discussed in greater detail in [6]. Section 3 reviews some of the definitions and results about the rigid-body kinematics of contact on which I build [8]. In Section 4, I give some new definitions and derive a set of equations, called the compliant contact equations, which describe how the centers of contact on the two surfaces evolve in response to a relative motion of the objects when the surfaces are allowed to deform. Section 5 discusses an example which illustrates the effect of compliance on the kinematics of contact. I measure the trajectory of the center of contact on a tactile sensor in response to a known motion and show how the results fit my model. Section 6 analyzes how two tasks discussed in [8] which are based on the rigid-body model of the kinematics of contact have been designed to be robust with respect to compliance. For the task of contour following I provide experimental results which confirm this analysis.

2 Mathematical Background

Notation Let C_{s_1} and C_{s_2} be two coordinate frames, where s_1 and s_2 are arbitrary subscripts. Then, $\vec{p}_{s_2 s_1}$ and $R_{s_2 s_1}$ denote the position and orientation of C_{s_1} relative to C_{s_2}. Furthermore, $\vec{v}_{s_2 s_1} = R^T_{s_2 s_1}\dot{\vec{p}}_{s_2 s_1}$ and $\Omega_{s_2 s_1} = R^T_{s_2 s_1}\dot{R}_{s_2 s_1}$ are the translational velocity and rotational velocity of C_{s_1} relative to C_{s_2}. The vector form of angular velocity is denoted by $\vec{\omega}_{s_2 s_1}$.

Proposition 1 *Consider three coordinate frames C_1, C_2 and C_3. The following relation exists between their relative velocities*

$$\vec{v}_{13} = R^T_{23}\vec{v}_{12} + R^T_{23}\Omega_{12}\vec{p}_{23} + \vec{v}_{23} \tag{1}$$

$$\Omega_{13} = R^T_{23}\Omega_{12}R_{23} + \Omega_{23} \tag{2}$$

Proof The proof is given in [8] and elsewhere.

Definition 1 A *coordinate patch* S_o for a surface $S \subset \Re^3$ is an open, connected subset of S with the following property: there exists an open subset U of $\Re^2$ and an invertible map $f : U \to S_o \subset \Re^3$ such that the partial derivatives $f_u(\vec{u})$ and $f_v(\vec{u})$ are linearly independent for all $\vec{u} = (u, v) \in U$. The pair (f, U) is called a *coordinate system* for S_o. The *coordinates* of a point $s \in S_o$ are $(u, v) = f^{-1}(s)$. A *2-manifold embedded in* $\Re^3$ (which we henceforth call a *manifold*) is a surface $S \subset \Re^3$ which can be written $S = \bigcup_{i=1}^n S_i$, where the S_i's are coordinate patches for S. The set $\{S_i\}_{i=1}^n$ is called an *atlas* for S.

Definition 2 A *Gauss map* (or *normal map*) for a manifold S is a continuous map $g : S \to S^2 \subset \Re^3$ such that for every $s \in S$, $g(s)$ is perpendicular to S at s. (Recall that S^2 is the unit sphere.) An *orientable* manifold S is one for which a Gauss map exists. When S is the surface of a solid object, we call the Gauss map which points outward the *outward normal map*.

Definition 3 Consider a manifold S with Gauss map g, a coordinate patch S_o for S, and a coordinate system (f, U) for S_o. The coordinate system (f, U) is *orthogonal* if $f_u(\vec{u}) \cdot f_v(\vec{u}) = 0$ for all $\vec{u} \in U$. When (f, U) is orthogonal, we can define the *normalized Gauss frame* at a point $\vec{u} \in U$ as the coordinate frame with origin at $f(\vec{u})$ and coordinate axes

$$\vec{x}(\vec{u}) = f_u(\vec{u})/\|f_u(\vec{u})\| \tag{3}$$

$$\vec{y}(\vec{u}) = f_v(\vec{u})/\|f_v(\vec{u})\| \tag{4}$$

$$\vec{z}(\vec{u}) = g(f(\vec{u})) \tag{5}$$

Note that the coordinate axes are functions mapping U to $\Re^3$. We call an orthogonal coordinate system (f, U) *right-handed* if its induced normalised Gauss frame is everywhere right-handed.

Note For any coordinate patch with an associated Gauss map there exists a right-handed, orthogonal coordinate system.

Definition 4 Consider a manifold S with Gauss map g, coordinate patch S_o, and orthogonal coordinate system (f, U). At a point $s \in S_o$, the *curvature form* K is defined as the 2x2 matrix

$$K = [\vec{x}(\vec{u}), \vec{y}(\vec{u})]^T [\vec{z}_u(\vec{u})/\|f_u(\vec{u})\|, \vec{z}_v(\vec{u})/\|f_v(\vec{u})\|] \tag{6}$$

*The research for this paper was performed while at the Division of Applied Sciences of Harvard University under the supervision of Roger W. Brockett. Financial support for this research was provided by AFOSR-85-0187 and NSF grants MEA-83-18972 and ECF-81-21428.

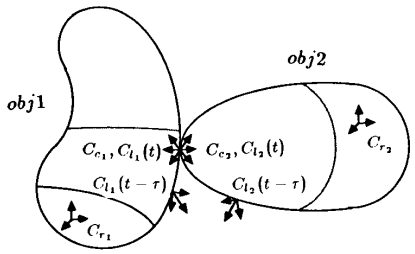

Figure 1: The coordinate systems (no compliance)

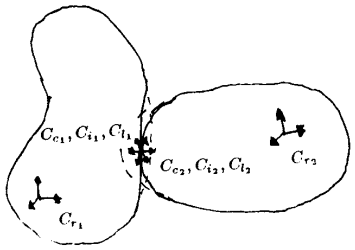

Figure 2: The coordinate systems (with compliance)

where $\vec{u} = f^{-1}(s)$. The *torsion form* T at s is the 1x2 matrix

$$T = \vec{y}(\vec{u})^T [\vec{x}_u(\vec{u})/\|f_u(\vec{u})\|, \vec{x}_v(\vec{u})/\|f_v(\vec{u})\|] \tag{7}$$

We define the *metric* M at s as the 2x2 diagonal matrix

$$M = \text{diag}(\|f_u(\vec{u})\|, \|f_v(\vec{u})\|) \tag{8}$$

An example illustrating all these definitions is given in [8].

3 The Kinematics of Contact

We now consider two rigid objects which move while maintaining contact with each other. Rigid bodies will generally make contact at isolated points rather than over areas of their surfaces. In this section we investigate the motion of one of these points of contact across the surfaces of the objects in response to a relative motion of the objects.

Call the objects $obj1$ and $obj2$. Choose reference frames C_{r_1} and C_{r_2} fixed relative to $obj1$ and $obj2$ respectively. Let $S_1 \subset \Re^3$ and $S_2 \subset \Re^3$ be the embeddings of the surfaces of $obj1$ and $obj2$ relative to C_{r_1} and C_{r_2} respectively. The surfaces S_1 and S_2 are orientable manifolds. Let g_1 and g_2 be the outward normal maps for S_1 and S_2. Choose atlases $\{S_{1_i}\}_{i=1}^{n_1}$ and $\{S_{2_j}\}_{j=1}^{n_2}$ for S_1 and S_2. Let (f_{1_i}, U_{1_i}) be an orthogonal, right-handed coordinate system for S_{1_i} with normal map g_1. Similarly, let (f_{2_j}, U_{2_j}) be an orthogonal, right-handed coordinate system for S_{2_j} with g_2.

Let $c_1(t) \in S_1$ and $c_2(t) \in S_2$ be the positions at time t of the point of contact relative to C_{r_1} and C_{r_2} respectively. In general, $c_1(t)$ will not remain in a single coordinate patch of the atlas $\{S_{1_i}\}_{i=1}^{n_1}$ for all time and likewise for $c_2(t)$ and the atlas $\{S_{2_j}\}_{j=1}^{n_2}$. Therefore, we restrict our attention to an interval I such that $c_1(t) \in S_{1_i}$ and $c_2(t) \in S_{2_j}$ for all $t \in I$ and some i and j. The coordinate systems (f_{1_i}, U_{1_i}) and (f_{2_j}, U_{2_j}) induce a normalized Gauss frame at all points in S_{1_i} and S_{2_j}. We define the contact frames, C_{c_1} and C_{c_2}, as the coordinate frames which coincide with the normalized Gauss frames at $c_1(t)$ and $c_2(t)$ respectively for all $t \in I$. We also define a continuous family of coordinate frames, two for each $t \in I$, as follows. Let the local frames at time t, $C_{l_1}(t)$ and $C_{l_2}(t)$, be the coordinate frames fixed relative to C_{r_1} and C_{r_2} respectively which coincide at time t with the normalized Gauss frames at $c_1(t)$ and $c_2(t)$ (see Figure 1).

We now define the parameters which describe the five degrees of freedom for the motion of the point of contact. The coordinates of the point of contact relative to the coordinate systems (f_{1_i}, U_{1_i}) and (f_{2_j}, U_{2_j}) are given by $\vec{u}_1(t) = f_{1_i}^{-1}(c_1(t)) \in U_{1_i}$ and $\vec{u}_2(t) = f_{2_j}^{-1}(c_2(t)) \in U_{2_j}$. These account for four degrees of freedom. The final parameter is the angle of contact, $\psi(t)$, which is defined as the angle between the x axes of C_{c_1} and C_{c_2}. We choose the sign of ψ so that a rotation of C_{c_1} through angle $-\psi$ around its z axis alligns the x axes.

We describe the motion of $obj1$ relative to $obj2$ at time t using the local coordinate frames, $C_{l_1}(t)$ and $C_{l_2}(t)$. Let v_x, v_y and v_z be the components of translational velocity of $C_{l_1}(t)$ relative to $C_{l_2}(t)$ at time t. Similarly, let ω_x, ω_y and ω_z be the components of rotational velocity. Then, v_x, v_y, v_z, ω_x, ω_y and ω_z provide the six degrees of freedom for the relative motion between the objects.

The symbols K_1, T_1 and M_1 represent respectively the curvature form, torsion form, and metric at time t at the point $c_1(t)$ relative to the coordinate system (f_{1_i}, U_{1_i}). We can analogously define K_2, T_2 and M_2. We also let

$$R_\psi = \begin{bmatrix} \cos\psi & -\sin\psi \\ -\sin\psi & -\cos\psi \end{bmatrix} \qquad \tilde{K}_2 = R_\psi K_2 R_\psi \tag{9}$$

Call $K_1 + \tilde{K}_2$ the *relative curvature form.*

Theorem 1 *At a point of contact, if the relative curvature form is invertible, then the point of contact and angle of contact evolve according to*

$$\dot{\vec{u}}_1 = M_1^{-1}(K_1 + \tilde{K}_2)^{-1}\left(\begin{bmatrix} -\omega_y \\ \omega_x \end{bmatrix} - \tilde{K}_2 \begin{bmatrix} v_x \\ v_y \end{bmatrix}\right) \tag{10}$$

$$\dot{\vec{u}}_2 = M_2^{-1} R_\psi (K_1 + \tilde{K}_2)^{-1}\left(\begin{bmatrix} -\omega_y \\ \omega_x \end{bmatrix} + K_1 \begin{bmatrix} v_x \\ v_y \end{bmatrix}\right) \tag{11}$$

$$\dot{\psi} = \omega_z + T_1 M_1 \dot{\vec{u}}_1 + T_2 M_2 \dot{\vec{u}}_2 \tag{12}$$

$$0 = v_z \tag{13}$$

Proof The proof is given in [8].

We call Equations 10-13 the *contact equations.*

4 Adding Compliance

We now show how to generalize this last result to allow for objects which are not rigid bodies. One important difference is that the idealization of point contact will in general not hold. Instead, there will be an area of contact. We are interested in its position as a function of time on the surfaces of the objects. We define the *center of contact* to be the point in the area of contact at which the torque is normal to the surface. We let the position of the center of contact represent the position of the area of contact. Hence, the center of contact for the compliant case is the analogue of the point of contact for the rigid-body case.

We also need to make some new definitions of coordinate systems and coordinate frames. For each time t, let $S_{d_1}(t)$ and $S_{d_2}(t)$ be the embeddings of the deformed surfaces relative to C_{r_1} and C_{r_2} respectively. There are functions $d_1(t) : S_1 \to S_{d_1}(t)$ and $d_2(t) : S_2 \to S_{d_2}(t)$ which map points on the undeformed surfaces to their positions under deformation. Let $f_{d_1}(t) = d_1(t) \circ f_{1_i}$ and $f_{d_2}(t) = d_2(t) \circ f_{2_j}$. The coordinate systems (f_{1_i}, U_{1_i}) and (f_{2_j}, U_{2_j}) for S_{1_i} and S_{2_j} respectively are mapped into coordinate systems $(f_{d_1}(t), d_1(t)(U_{1_i}))$ and $(f_{d_2}(t), d_2(t)(U_{2_j}))$ for coordinate patches of $S_{d_1}(t)$ and $S_{d_2}(t)$. These coordinate systems for the deformed surfaces will in general not be orthogonal.

Let $c_1(t) \in S_{d_1}(t)$ and $c_2(t) \in S_{d_2}(t)$ be the positions of the center of contact relative to C_{r_1} and C_{r_2} respectively. The coordinates of the center of contact are $\vec{u}_1(t) = f_{d_1}(t)^{-1}(c_1(t))$ and $\vec{u}_2(t) =$

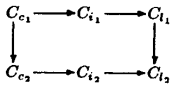

Figure 3: Paths from C_{c_1} to C_{l_2}

$f_{d_2}(t)^{-1}(c_2(t))$. We redefine C_{c_1}, the contact frame from $obj1$, as follows: at time t, the z axis is outwardly normal to $S_{d_1}(t)$, the x axis is $(f_{d_1}(t))_u/\|(f_{d_1}(t))_u\|$ evaluated at $c_1(t)$ and the y axis is the cross-product of the z axis and the x axis. (This unfortunately introduces assymetry between the x and y directions.) Define C_{c_2} similarly. $C_{l_1}(t)$ and $C_{l_2}(t)$ are defined the same as for the rigid-body case: They are the coordinate frames fixed relative to C_{r_1} and C_{r_2} respectively which coincide with C_{c_1} and C_{c_2} at time t. We next define two new families of coordinate frames, $C_{i_1}(t)$ and $C_{i_2}(t)$, called the intermediate coordinate frames. To get $C_{i_1}(t)$, transform the surface S_1 and its atlas by a rigid-body transformation such that the normalized Gauss frame at $\vec{u}_1(t)$ coincides with $C_{c_1}(t)$. Then, $C_{i_1}(t)$ is at all times t_0 the normalized Gauss frame at $\vec{u}_1(t_0)$ for this transformed surface (see Figure 2).

The compliance velocities $\vec{v}_{c_1}$ and $\vec{\omega}_{c_1}$ for $obj1$ at time t are defined as the translational and angular velocities of C_{c_1} relative to $C_{i_1}(t)$. The compliance velocities, $\vec{v}_{c_2}$ and $\vec{\omega}_{c_2}$ are defined similarly. The components of $\vec{v}_{c_1}$ and $\vec{\omega}_{c_1}$ are $v_{c_{1x}}$, $v_{c_{1y}}$, $v_{c_{1z}}$, $\omega_{c_{1x}}$, $\omega_{c_{1y}}$, and $\omega_{c_{1z}}$, and similarly for $\vec{v}_{c_2}$ and $\vec{\omega}_{c_2}$. Define the total velocities $\vec{v}_t$ and $\vec{\omega}_t$ as

$$\vec{v}_t = \begin{bmatrix} v_{t_x} \\ v_{t_y} \\ v_{t_z} \end{bmatrix} = \begin{bmatrix} v_x \\ v_y \\ v_z \end{bmatrix} + \begin{bmatrix} v_{c_{1x}} \\ v_{c_{1y}} \\ v_{c_{1z}} \end{bmatrix} - \begin{bmatrix} R_\psi \begin{bmatrix} v_{c_{2x}} \\ v_{c_{2y}} \end{bmatrix} \\ -v_{c_{2z}} \end{bmatrix} \quad (14)$$

$$\vec{\omega}_t = \begin{bmatrix} \omega_{t_x} \\ \omega_{t_y} \\ \omega_{t_z} \end{bmatrix} = \begin{bmatrix} \omega_x \\ \omega_y \\ \omega_z \end{bmatrix} + \begin{bmatrix} \omega_{c_{1x}} \\ \omega_{c_{1y}} \\ \omega_{c_{1z}} \end{bmatrix} - \begin{bmatrix} R_\psi \begin{bmatrix} \omega_{c_{2x}} \\ \omega_{c_{2y}} \end{bmatrix} \\ -\omega_{c_{2z}} \end{bmatrix} \quad (15)$$

ψ continues to be defines as the angle between the x axes of the contact frames.

Theorem 2 *At an area of contact, if the relative curvature form is invertible, then the centers of contact and angle of contact evolve according to*

$$\dot{\vec{u}}_1 = M_1^{-1}(K_1 + \tilde{K}_2)^{-1}(\begin{bmatrix} -\omega_{t_y} \\ \omega_{t_x} \end{bmatrix} - \tilde{K}_2 \begin{bmatrix} v_{t_x} \\ v_{t_y} \end{bmatrix}) \quad (16)$$

$$\dot{\vec{u}}_2 = M_2^{-1} R_\psi (K_1 + \tilde{K}_2)^{-1}(\begin{bmatrix} -\omega_{t_y} \\ \omega_{t_x} \end{bmatrix} + K_1 \begin{bmatrix} v_{t_x} \\ v_{t_y} \end{bmatrix}) \quad (17)$$

$$\dot{\psi} = \omega_{t_z} + T_1 M_1 \dot{\vec{u}}_1 + T_2 M_2 \dot{\vec{u}}_2 \quad (18)$$

$$0 = v_{t_z} \quad (19)$$

Proof In Figure 3 are shown two paths from coordinate frame C_{c_1} to coordinate frame C_{l_2}. We define taking a step along a path to mean performing the following recursive procedure: Express the motion parameters of C_{c_1} relative to the new coordinate frame by applying Proposition 1 to the motion parameters of C_{c_1} relative to the old coordinate frame and motion parameters of the old coordinate frame relative to the new one. Following each path will allow us to express the motion parameters of C_{c_1} relative to C_{l_2} in two different ways.

For each step in the paths, we now give the motion parameters of the old coordinate frame relative to the new one. These values either come straight from the definitions given above or have derivations completely analogous to derivations in [8].

$$C_{c_1} \to C_{c_2} \quad : \quad R = \begin{bmatrix} R_\psi & 0 \\ 0 & -1 \end{bmatrix}, \vec{p} = 0, \vec{v} = 0$$
$$\Omega = \begin{bmatrix} 0 & -\psi & 0 \\ \psi & 0 & 0 \\ 0 & 0 & 0 \end{bmatrix} \quad (20)$$

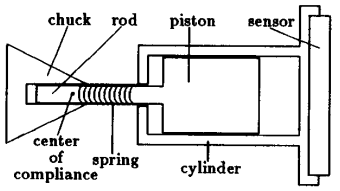

Figure 4: Device which holds the sensor

$$C_{c_2} \to C_{i_2} \quad : \quad R = I, \vec{p} = 0, \vec{v} = \begin{bmatrix} v_{c_{2x}} \\ v_{c_{2y}} \\ v_{c_{2z}} \end{bmatrix}$$
$$\Omega = \begin{bmatrix} 0 & -\omega_{c_{2z}} & \omega_{c_{2y}} \\ \omega_{c_{2z}} & 0 & -\omega_{c_{2x}} \\ -\omega_{c_{2y}} & \omega_{c_{2x}} & 0 \end{bmatrix} \quad (21)$$

$$C_{i_2} \to C_{l_2} \quad : \quad R = I, \vec{p} = 0, \vec{v} = \begin{bmatrix} M_2 \dot{\vec{u}}_2 \\ 0 \end{bmatrix}$$
$$\Omega = \begin{bmatrix} 0 & -T_2 M_2 \dot{\vec{u}}_2 & K_2 M_2 \dot{\vec{u}}_2 \\ T_2 M_2 \dot{\vec{u}}_2 & 0 & \\ & -(K_2 M_2 \dot{\vec{u}}_2)^t & 0 \end{bmatrix} \quad (22)$$

$$C_{c_1} \to C_{i_1} \quad : \quad R = I, \vec{p} = 0, \vec{v} = \begin{bmatrix} v_{c_{1x}} \\ v_{c_{1y}} \\ v_{c_{1z}} \end{bmatrix}$$
$$\Omega = \begin{bmatrix} 0 & -\omega_{c_{1z}} & \omega_{c_{1y}} \\ \omega_{c_{1z}} & 0 & -\omega_{c_{1x}} \\ -\omega_{c_{1y}} & \omega_{c_{1x}} & 0 \end{bmatrix} \quad (23)$$

$$C_{i_1} \to C_{l_1} \quad : \quad R = I, \vec{p} = 0, \vec{v} = \begin{bmatrix} M_1 \dot{\vec{u}}_1 \\ 0 \end{bmatrix}$$
$$\Omega = \begin{bmatrix} 0 & -T_1 M_1 \dot{\vec{u}}_1 & K_1 M_1 \dot{\vec{u}}_1 \\ T_1 M_1 \dot{\vec{u}}_1 & 0 & \\ & -(K_1 M_1 \dot{\vec{u}}_1)^t & 0 \end{bmatrix} \quad (24)$$

$$C_{l_1} \to C_{l_2} \quad : \quad R = \begin{bmatrix} R_\psi & 0 \\ 0 & -1 \end{bmatrix}, \vec{p} = 0, \vec{v} = \begin{bmatrix} v_x \\ v_y \\ v_z \end{bmatrix}$$
$$\Omega = \begin{bmatrix} 0 & -\omega_x & \omega_y \\ \omega_x & 0 & -\omega_z \\ -\omega_y & \omega_z & 0 \end{bmatrix} \quad (25)$$

The rest of the proof is just substituting into Proposition 1 four times, setting equal the two different expressions for the translational and rotational velocities of C_{c_1} relative to C_{l_2}, and performing algebraic manipulation. These steps are left to the reader.

5 An Example

I have performed a series of experiments which measure how the point of contact moves across the surface of a tactile sensor in response to different motions of the sensor relative to an object [7]. The experimental setup was as follows. The tactile sensor used is manufactured by Barry-Wright Corporation and is described in (Wright 1983). It has a 16x16 grid of sensing elements with inter-element spacing of 0.1". One notable feature is the high variance of sensitivity among sensing elements. This could have been compensated for in software, but I chose not to do so to prove the robustness of the center of contact calculation.

To hold the sensor, we built the device pictured in Figure 4. It allows compliance translationally in the direction normal to the sensor surface and rotationally around axes parallel to the sensor surface through the center of compliance. The distance from the center of compliance to the sensor surface is approximately 7".

The robot used to maneuver the sensor is an Automatix AID600. Using the control software that Automatix supplied, the robot could

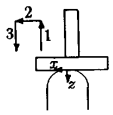

Figure 5: Eliminating frictional effects

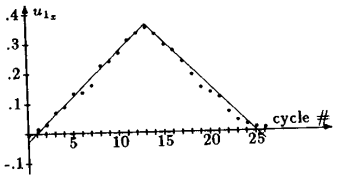

Figure 6: Pure translation without friction

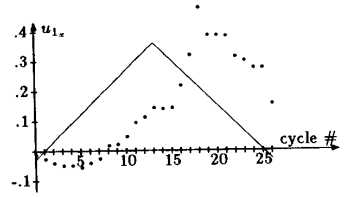

Figure 7: Pure translation with friction

only move from point to point or follow a prespecified path of points.

The object which the sensor contacts is fixed with respect to the base of the robot and is nearly rigid (at least for our purposes). Its shape is roughly spherical with radius of curvature approximately 3".

Since the undeformed sensor surface is flat, we can coordinatize its embedding S_1 using a Cartesian coordinate system, with u being the distance in sensing elements along one edge of the sensor surface and v the distance along an adjacent edge. Then, $K_1 = 0$, $T_1 = 0$ and $M_1 = 0.1I$, where 0.1 is the inter-element spacing. The curvature of the fixed object is roughly $\frac{1}{3}I$.

Because the sensor surface is essentially flat, the center of contact is the centroid of the normal forces. We calculate the approximate position of the center of contact as

$$\vec{u}_1 = \begin{bmatrix} u_{1_x} \\ u_{1_y} \end{bmatrix} = \frac{\sum_{u=0}^{15}\sum_{v=0}^{15} m(u,v) \begin{bmatrix} u \\ v \end{bmatrix}}{\sum_{u=0}^{15}\sum_{v=0}^{15} m(u,v)} \tag{26}$$

where $m(u,v)$ is the response of the sensing element at position (u,v).

Since the fixed object is rigid, its compliance velocities are $\vec{v}_{c_2} = \vec{\omega}_{c_2} = 0$. The compliance velocities of the sensor are approximately

$$\vec{v}_{c_1} = \begin{bmatrix} l\dot{\phi}_y \\ -l\dot{\phi}_x \\ \dot{l} \end{bmatrix} \qquad \vec{w}_{c_1} = \begin{bmatrix} \dot{\phi}_x \\ \dot{\phi}_y \\ 0 \end{bmatrix} \tag{27}$$

where l is the distance of the sensor surface from the center of compliance and ϕ_x and ϕ_y are the angular displacements of the sensor around the center of compliance about axes parallel to the x and y directions on the sensor surface respectively. This implies that $\omega_{c_{1x}} = -v_{c_{1y}}/l$ and $\omega_{c_{1y}} = v_{c_{1x}}/l$. Note that we can measure l but must infer ϕ_x and ϕ_y from the motion of the point of contact.

We use the standard Coulomb model of friction. Static friction acts so as to not let the surfaces slip. This translates into the constraint $v_{t_x} = v_{t_y} = 0$. Since $v_{t_x} = v_x + v_{c_{1x}} + v_{c_{2x}}$ and $v_{c_{2x}} = 0$, then $v_{c_{1x}} = -v_x$. Similarly, $v_{c_{1y}} = -v_y$. Then, according to our model of compliance, $\omega_{c_{1y}} = -v_x/l$ and $\omega_{c_{1x}} = v_y/l$.

Static friction holds until the tangential force needed to maintain

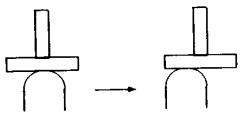

Figure 8: Initial translation without friction

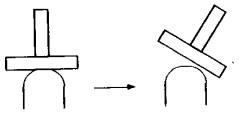

Figure 9: Initial translation with friction

the constraint $v_{t_x} = v_{t_y} = 0$ is greater than κ_s, the static coefficient of friction, times the normal force. At this point, slippage occurs and kinetic friction replaces static friction. Kinetic friction acts so that the magnitude of the tangential force is κ_k, the kinetic coefficient of friction, times the normal force. Kinetic friction holds until $v_{t_x} = v_{t_y} = 0$, at which point static friction occurs.

The first experiment I performed examined the system behavior under pure translation. Because of the limitations of the robot control, I used a measure-then-move cycle, first measuring the position of the center of contact on the sensor surface, then repositioning the robot, and then measuring again. I made two runs using two different motion strategies. The first moved the robot so as to translate the sensor $\Delta x = -0.03''$ in the x direction (the direction pointing towards increasing u) for 13 cycles and then $\Delta x = 0.03''$ for 13 cycles. The second performed the same basic motion but eliminated frictional effects using the procedure illustrated in Figure 5: 1) move the sensor away from the object so that contact is broken, 2) translate the sensor by Δx, 3) move the sensor back into contact with the object. The results are pictured in Figures 6 and 7.

We now calculate the theoretical predictions derived from our model. In the case when frictional effects are removed, $v_{c_{1x}} = v_{c_{1y}} = 0$. Substituting into Equation 16 gives

$$\Delta\vec{u}_1 = \begin{bmatrix} -\Delta x/0.1 \\ 0 \end{bmatrix} \tag{28}$$

This is the same result which we would get using the rigid-body model. Figure 6 shows how close the theoretical prediction corresponds with the experimental results.

We next examine the case when frictional effects are present. The motion of the center of contact has four phases.

Phase 1: Static friction acts exclusively. Hence, $v_{t_x} = v_{t_y} = 0$. In response to a translation through Δx, $\omega_{t_x} = 0$ and $\omega_{t_y} = -\Delta x/l \approx -\Delta x/7$. Substituting into Equation 16 gives

$$\Delta\vec{u}_1 \approx \begin{bmatrix} \Delta x/(7 \cdot 0.1) \\ 0 \end{bmatrix} \tag{29}$$

When $\Delta x = -0.03$, $\Delta u_{1_x} \approx -0.04$. We see in Figure 7 that this phase lasts for approximately the first four steps. Note that the center of contact moves in the opposite direction than it does without frictional effects. Figures 8 and 9 illustrate why this happens.

Phase 2: The forces needed to maintain the constraint $v_{t_x} = v_{t_y} = 0$ are too great and thus static friction gives way to kinetic friction. Since the robot stops after every step, static friction has a chance to take hold between each cycle. However, soon after the robot moves a little more, kinetic friction takes over again. This continual switching between kinetic and static friction makes a step-by-step prediction difficult. On average during this interval, the compliance velocity is zero, and thus $\Delta\vec{u}_1 = \Delta x/0.1$. This phase lasts from step 5 to step 13.

Phases 3 and 4 are similar to phases 1 and 2 respectively.

A second experiment was done to test how well the model predicts system behavior for pure rotation of the sensor relative to the object. Two trials were performed, one using the method described above to eliminate frictional effects and the other leaving in the frictional effects.

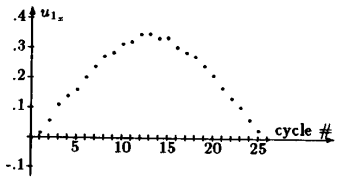

Figure 10: Pure rotation without friction

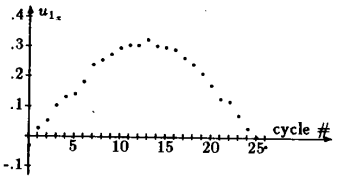

Figure 11: Pure rotation with friction

Each trial consisted of 26 steps, the first 13 steps with $\Delta\theta_y = -0.01$ and the second 13 with $\Delta\theta_y = 0.01$. Since $v_x = v_y = 0$, the static friction constraint $v_{t_x} = v_{t_y} = 0$ implies that $v_{c_{1x}} = v_{c_{1y}} = 0$. Hence, $\omega_{c_{1x}} = \omega_{c_{1y}} = 0$. So, compliance has no effect, and therefore the results of the two trials should be the same. In fact, we see from Figures 10 and 11 that the experiment agrees with the theoretical prediction. Substituting into Equation 16 gives $\Delta u_{1_x} = \frac{-3}{0.1}\Delta\theta_y$. This holds approximately in the experiments, and any deviations can be explained by errors in estimation of the curvature of the object (which is not perfectly spherical).

6 Manipulation Tasks

When designing manipulation tasks for a compliant environment, there are two possible approaches to dealing with compliance. One is to not include compliance in the model but to make the control closed-loop and have it compensate for the errors introduced by compliance. The other is to incorporate an understanding of the effects of compliance into the model on which the task design is based. In [8] there were manipulation tasks described which took each of these approaches: a method of contour following uses the first approach and a method of finding curvature uses the second.

In [8], I discussed a method of following the surface of an arbitrary unknown object with a tactile sensor. Based on my model of the rigid-body kinematics of contact, the proposed control laws steer the point of contact on the sensor surface to some desired point using closed-loop control to adapt to the unknown and changing curvature of the object and to damp out any errors due to deviations from the model. To test how well the control can compensate for the errors introduced by compliance, I conducted an experiment. The original control laws were designed to be run as a continuous servo loop. I adapted them for the measure-then-move experimental setup which I had [7]. With this set of control laws, I performed two experimental runs, one with friction and one without, using the method described in Section 5 to eliminate frictional effects. The two runs started with the same initial conditions. Figures 12 and 13 show the trajectory of the point of contact on the sensor surface as the control laws try to steer it to zero. Notice that there was not that great a performance drop with the addition of friction.

In [8] I described a method which uses active sensing to determine the curvature of an unknown object. The idea is to make small movements of the sensor and measure the change in the position of the point of contact. Substituting the results into Equation 10 gives an equation whose only unknown is the curvature of the object. This is inherently an open-loop procedure and is sensitive to any errors. To reduce the effects of compliance, we specify that the small sensor movements should

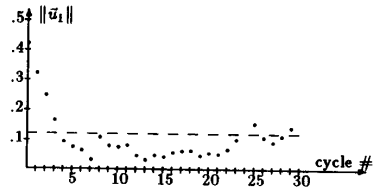

Figure 12: Contour following without friction

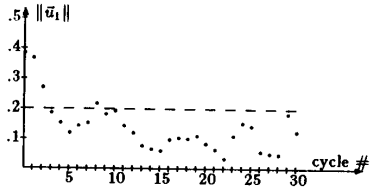

Figure 13: Contour following with friction

be purely rotational. Hence, there will be no frictional force causing the effects documented in Section 5. In general, understanding how compliance effects the kinematics of contact can help us design tasks to be robust with respect to compliance.

7 Conclusion

The kinematics of contact provide a powerful model on which to base design of manipulation tasks. Previous formulations of the kinematics of contact assumed rigidity for the objects. However, in the physical world, objects (including grasping surfaces) often have significant compliance. As shown by experiments I have described, compliance can cause large deviations from the rigid-body model. Therefore, I have derived an extension to the rigid-body kinematics of contact to include compliance. Using this new model, I have explained the results of the experiments. Finally, I have explored how to make manipulation applications based on my model of the kinematics of contact robust with respect to compliance. To illustrate the robustness of a contour following algorithm, I have presented the results of an experiment.

References

[1] Brockett, R.W. 1985. Robotic Hands with Rheological Surfaces. *Proc. 1985 IEEE Conf. on Robotics and Automation,* pp. 942-946.

[2] Cai, C. and B. Roth. 1987. On the spatial motion of rigid bodies with point contact. *Proc. 1987 IEEE Conf. on Robotics and Automation,* Raleigh, NC, pp. 686-695.

[3] Clark, J.J. 1988. A Magnetic Field Based Compliance Matching Sensor for High Resolution, High Compliance Tactile Sensing. *Proc. 1988 IEEE Conf. on Robotics and Automation,* Philadelphia, pp. 772-777.

[4] Cutkosky, M.R. and P.K. Wright. 1986. Friction, Stability and the Design of Robotic Fingers. *Int. J. Robotics Res.* 5(4):20-37.

[5] Fearing, R.S. and J.H. Hollerbach. 1985. Basic solid mechanics for tactile sensing. *Int. J. Robotics Res.* 4(3):40-54.

[6] Klingenberg, W. 1978. *A Course in Differential Geometry.* New York: Springer-Verlag.

[7] Montana, D.J. 1986. Tactile sensing and the kinematics of contact. Ph.D. Thesis, Division of Applied Sciences, Harvard University.

[8] Montana, D.J. 1988. The Kinematics of Contact and Grasp. *Int. J. Robotics Res.* 7(3):17-32.